



SCIENCE AND TECHNOLOGY ORGANIZATION  
CENTRE FOR MARITIME RESEARCH AND EXPERIMENTATION



**Reprint Series**

**CMRE-PR-2019-106**

# **Ambiguity reduction of underwater targets in framework of topic modeling**

Jüri Sildam, Kevin D. LePage

June 2019

Originally published in:

18th International Conference on Information Fusion, 6-9 July 2015,  
Washington DC, USA, pp. 2017-2024.

## About CMRE

The Centre for Maritime Research and Experimentation (CMRE) is a world-class NATO scientific research and experimentation facility located in La Spezia, Italy.

The CMRE was established by the North Atlantic Council on 1 July 2012 as part of the NATO Science & Technology Organization. The CMRE and its predecessors have served NATO for over 50 years as the SACLANT Anti-Submarine Warfare Centre, SACLANT Undersea Research Centre, NATO Undersea Research Centre (NURC) and now as part of the Science & Technology Organization.

CMRE conducts state-of-the-art scientific research and experimentation ranging from concept development to prototype demonstration in an operational environment and has produced leaders in ocean science, modelling and simulation, acoustics and other disciplines, as well as producing critical results and understanding that have been built into the operational concepts of NATO and the nations.

CMRE conducts hands-on scientific and engineering research for the direct benefit of its NATO Customers. It operates two research vessels that enable science and technology solutions to be explored and exploited at sea. The largest of these vessels, the NRV Alliance, is a global class vessel that is acoustically extremely quiet.

CMRE is a leading example of enabling nations to work more effectively and efficiently together by prioritizing national needs, focusing on research and technology challenges, both in and out of the maritime environment, through the collective Power of its world-class scientists, engineers, and specialized laboratories in collaboration with the many partners in and out of the scientific domain.



**Copyright © IEEE, 2015.** NATO member nations have unlimited rights to use, modify, reproduce, release, perform, display or disclose these materials, and to authorize others to do so for government purposes. Any reproductions marked with this legend must also reproduce these markings. All other rights and uses except those permitted by copyright law are reserved by the copyright owner.

**NOTE:** The CMRE Reprint series reprints papers and articles published by CMRE authors in the open literature as an effort to widely disseminate CMRE products. Users are encouraged to cite the original article where possible.

---

# Ambiguity Reduction of Underwater Targets in Framework of Topic Modeling

**Jüri Sildam**  
 NATO STO CMRE  
 La Spezia, Italy  
 Juri.Sildam@cmre.nato.int

**Kevin D. LePage**  
 NATO STO CMRE  
 La Spezia, Italy  
 Kevin.LePage@cmre.nato.int

*Abstract - an unsupervised track classification approach based on appropriate discriminative and aggregative features derived from beamformed and normalized matched-filtered data is applied to sonar multistatic tracking and extended to include discretised track velocity and heading rate. A clustering algorithm based on the Latent Dirichlet Allocation model is proposed. It is demonstrated how low-level, highly variable and non-stationary data components can be combined through an increased abstraction level with higher level kinematic tracking features. Improved discrimination of tracks associated with both stationary and moving scatterers is demonstrated.*

**Keywords:** multistatic tracking, data aggregation and clustering, track classification, Latent Dirichlet Allocation

## 1 Introduction

In the context of anti-submarine warfare (ASW) one of the central goals of autonomous underwater vehicles (AUVs) is detection and tracking of underwater targets. For multistatic sonar networks a decision regarding the presence or absence of a target (DPAT) can be carried out at increasing information processing levels until confidence sufficient for making the DPAT is reached.

At the lowest level, DPAT is carried out using a single detection or contact and is based on some form of signal-to-noise ratio (SNR) test. Usually at this level, to prevent incorrect rejection of detections related to a target, a number of false detections not related to the target are accepted and passed to the tracking level where contacts are used to form tracks. At the tracking level “track before detect” approaches may be used for DPAT. The DPAT may then be passed to higher levels within a data fusion framework if at the tracking level the number of false tracks remains too high.

One of the questions that has not obtained much attention in DPAT is as follows: “Have we maximized the amount of useful information that are available from low (sensor) level processing that should be passed to the higher DPAT levels?” In other words, are we discarding information at low levels that can be important during high-level decision making processes?

One of the obstacles preventing a direct real-world validated answer to this question is the uncertainty of the ground truth information (e.g. uncertainty of target acoustic response due to active interrogation) conveyed through the uncertainty of contact and/or track labeling. For example, track labeling is straightforward in cases of high SNR contacts that are associated to a track aligned with a known target trajectory, for instance by lying at a close distance from the known trajectory. However, track labeling is less obvious in cases where several tracks associated with low SNR contacts coexist in a proximity of the target. In this case, labelling the track or the contact nearest to the target as being target related is not necessarily the correct choice.

The problem of track labelling uncertainty can be addressed by unsupervised track grouping into patterns such that the different patterns correspond to the different types of false tracks of target-like-objects (TLOs) and to the tracks related to target (T). Visualization of such patterns provides a way of outlining not only the track patterns corresponding to T using uncertain ground truth information but also the tentative TLO patterns which lack ground truth information. The TLO patterns can be then be revisited for closer inspection and analysis. Building a statistical model enabling the real-time modeling of T-TLO feature patterns by maximizing the relative distance between their respective patterns via improvement of feature extraction from all levels of information is a direction taken in this work.

Typically the information that is passed from the lowest processing level to the tracking level is limited to the kinematic features such as spatial coordinates of contacts, and if possible also closing velocity estimates. The non-kinematic features already used directly for contact detection (e.g. SNR) have a limited additional DPAT value.

In this work we are interested in DPAT improvement including decisions about stationary targets through a combination of the low level non-kinematic and the track level kinematic features (that according to [11] correspond respectively to Levels 0 and 1) that can be used both in fully automated or in human-in-the-loop decision making. Our work differs from other work in this area by its emphasis on the increased abstraction of low level multistatic sonar features that a) allow us to model the joint distributions of non-kinematic and kinematic features in a computationally efficient manner suitable for real-time underwater autonomous vehicles (AUVs), and b) provides a structured

approach for further DPAT improvement through the abstraction of other acoustic and non-acoustic sensor low-level features. In other words, we attempt to combine aspects of research from two practically independent communities, the first one having concentrated for more than last two decades on clutter related DPAT improvement using only contact level information (for a recent publication see e.g. [1]), and the second one having concentrated on the track-before-detect level approaches using basically kinematic features of contacts and tracks (including the ASW network based approaches that optimize also AUV path planning, see e.g. [2]). It should be stressed that in an ASW context a target is confirmed only after a visual target sighting or other non-ambiguous measurement, which in many cases is unachievable.

The results of this work, centered on track classification by integrating low-level and the high-level kinematic features, are built on our previous work [3] showing improved track classification using unsupervised clustering of aggregative discriminative low-level contact feature associated with tracks.

In the following section we first provide more details motivating the construction of extended features, followed by the description of features' construction. The feature construction section will be followed by a short description of Latent Dirichlet Allocation model used in this work for track clustering. Finally we will present the results followed by summary.

## 2 Point target detection

Typical detection of point targets by mid-frequency (MF) active sonars is “based on a relationship or ratio that exists between the desired and undesired portions of the received energy when some function of the sonar equipment such as detection or classification is performed” [4]. In practice, the undesired part of the received energy of time series of beamformed and matched filtered data (which we call noise) is estimated from the background of the portion of the time series in which the echo is embedded. Usually the background portion is extracted from the close vicinity (e.g. before and after) of the portion of time series that has been identified as the potential target echo.

Detectors can be divided into either binary detectors (BD) or multiclass detectors (MD) depending on whether classification of echoes is required or not. BDs are unambiguous only when targets of interest are the only objects giving rise to echoes.

To distinguish the detection errors that arise from incorrect noise-echo discrimination from those errors that arise from incorrect echo classification, we call erroneous detections either false alarms or ambiguous detections. Collectively all detections that pass an echo to background level test are called contacts. Each contact has a number of features associated to it: for instance a feature characterizing energy spread in vicinity of peak amplitude, or that contact's association to a track. In addition to the individual contact

features, a tracker can be used to associate contact and kinematic track features.

A typical active narrowband (NB) sonar contact detector does not carry out any echo classification but rather addresses the T-TLO discrimination problem through closing velocity measurements under the assumption that Ts move while TLOs are stationary. In the case of stationary or slowly moving Ts this approach either cannot be used or has limited value.

In previous work [3] we showed that T-TLO ambiguity can be reduced via track classification where a tracking algorithm acts as a contact associator forming sets of contacts. This track classification is based on an implicit assumption that in ASW T-TLO discrimination can be based on respective differences in recorded signal spread in the beam-number – bistatic-travel-time domain. Arguing that direct modeling of the causes underlying the spread of the signal amplitude envelope is problematic under constraints of real-time processing we introduced a *discriminative aggregative* feature, the Difference Entropy of Similarity Test (DEST), and model the DEST distribution in a framework of a generative model based on Dirichlet processes.

In the next sections we detail the motivation behind the DEST feature and show that it can be readily combined with higher level features, joint statistical modeling of which can lead to a further reduction of DPAT ambiguity.

## 3 Feature construction

### 3.1 Motivation for construction of high abstraction level features

Information about clutter and target can be obtained on bearings next to the bearing of a contact. At a low level i.e. at the level of received amplitudes, the respective information can change depending on the target – receiver distance (Fig. 1). While clutter may contribute significantly to signal energy on neighboring beams, so does imperfect spatial filtering of a recorded signal or any deviation from the array shape assumed during beam-forming. Resolving such causes via direct modeling may be problematic under the constraints of real-time processing.

An essential constraint preventing reliable T-TLO echo discrimination using solely lower level abstraction features obtained from active NB sonar operating in a variable environment with a constantly changing measurement geometry (i.e. under moving target and receiver assumptions) lies in the limited amount of stationary data that can be collected in a limited time-space window.

Another constraint typical to NB contact distributions closely related to the limit stated above is uncertainty of contact labelling *visa-vis* noise and T or TLO contacts. This uncertainty increases with decreasing signal-to-noise (SNR) ratio, and must be estimated from a limited amount of available independent data.

Using tracking algorithm that associate contacts with tracks uniquely and blindly (i.e. without explicit labelling) either as T or TLO, one can form respective sets of contacts.

It is desirable that the joint probability distribution of all features of associated contacts would be invariant to environmental changes, and that the parameters governing T-TLO probability distributions could be grouped into a relatively limited number of clusters so that parameters governing their respective partitions could reliably be learned from the available data.

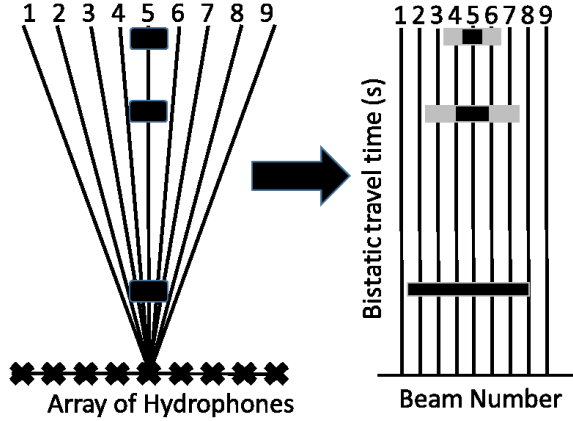


Fig. 1: Distribution of beams and TLO as seen from the array centre (left), and in beam-number – bistatic travel time space (right) (drawn after [5]).

Discriminative feature aggregation can be thought as a process of increasing feature abstraction level such that on the higher abstraction levels individual features can be modeled jointly with other features obtained by processing data from different sensors and/or by constructing independent features in addition to existing ones using the same sensors. For discrete features such a joint probability may be interpreted as a co-occurrence of different events or as a co-occurrence of a features meaningfulness of interpretation of which the meaningfulness of constructed features depends.

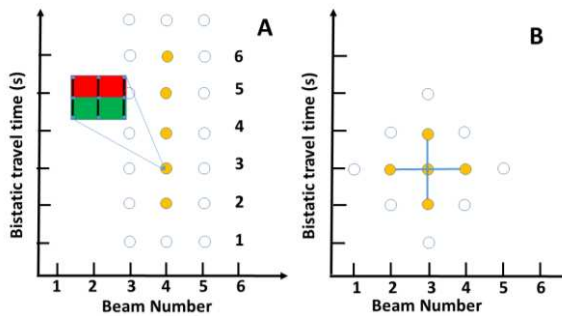


Fig. 2: low level feature estimation. A – MMD test. The two sets of time-series snippets are shown by the green and red boxes respectively. Yellow filled circles denote positions of estimated  $d$  values. B-DEST estimation. Blue solid lines connect  $d$  values used for DEST estimation shown by central filled circle.

Combinations of features meaningful to operators (e.g. distribution of track velocity and heading rate) with the

features the meaning of which is less apparent (such as DEST) is a way to increase operator confidence in DPAT. Such a combination also provides a way to fuse contextual information (i.e. in a sense of pattern recognition [12]) with the features extracted at high abstraction levels from the low level data streams of heterogeneous sensors, such as the Maximum Mean Discrepancy (MMD) entropy difference of passive acoustical sensors [6] [7], and provides a way to formalize information required for interactive decision making. For example a decision can be based on the following statement: “detection of the stationary object is based on a noise-like track velocity distribution, and by features characterizing the T signal spread, which exclude TLOs characterized by the signal spread associated with the side-lobes of direct blast”.

TABLE I

K	L	K	L	K	L
1	$\tilde{h}1$	13	d6	25	v11
2	$\tilde{h}2$	14	d7	26	a1
3	$\tilde{h}3$	15	v1	27	a2
4	$\tilde{h}4$	16	v2	28	a3
5	$\tilde{h}5$	17	v3	29	a4
6	$\tilde{h}6$	18	v4	30	a5
7	$\tilde{h}7$	19	v5	31	a6
8	d1	20	v6	32	a7
9	d2	21	v7		
10	d3	22	v8		
11	d4	23	v9		
12	d5	24	v10		

K – Feature number, L - feature label consisting from tag (e.g.  $\tilde{h}$ ) and relative number of feature tag (e.g.2); Tag labels:  $\tilde{h}$  – entropy difference of  $d$  distributions;  $d$  – discretized value of Maximum Mean Discrepancy test;  $v$  – target velocity (m/s) {0,0.5,1,1.5,2,2.5,3,3.5,4,4.5,5,0};  $a$  – azimuth change rate (Deg/s) {0,0.17,0.33,0.50,0.67,0.83,1,0}  
Vocabulary of features -  $W = \{\tilde{h}1, \dots, \tilde{h}7, d1, \dots, d7, v1, \dots, v11, a1, \dots, a7\}$

### 3.2 Low level features

Low level features are constructed from preprocessed towed array sonar data. In this work we will consider two low level features: 1) the discretized values of MMD test [6] (Table I, features  $\{d1, \dots, d7\}$ ), and 2) the DEST or the difference of entropies of MMD distributions estimated along and across contact bearing (Table I, features  $\{\tilde{h}1, \dots, \tilde{h}7\}$ ). Details about these two features are given in [3] and in the Appendix.

The hierarchical aggregative nature of the DEST feature is illustrated in Fig.3. At the lower level ( $\mathbf{x}$ ), the blue filled circles correspond to the time snippets of normalized data vectors. The next level ( $\mathbf{d}$ ) shown by the yellow filled circles corresponds to the discretized MMD values estimated along the beam (e.g. beam  $j=4$ , time indices  $i = \{2, \dots, 6\}$  in Fig. 2A; Table 1, features 8-14). The DEST is based on the two histograms of MMD discretized output estimated along and across the beams of a contact (Fig. 2B). These histograms are used for entropy estimation along ( $h_t$ ) and across ( $h_b$ ) beams. The DEST feature is defined as entropy difference  $\tilde{h} = h_t - h_b$ . In this way the DEST construction performs a triple aggregation of the relative changes around of each contact.

By moving the TB window to the four cardinal directions around the central contact (Figure 2B) the DEST estimation is repeated four times (four filled yellow circles around the contact in the centre). The five resulting DEST values are then sorted into a seven bin histogram (Table I, features 1-7).

### 3.3 Track level features

In addition to the low level MMD and DEST features associated with contacts, we estimate the velocity and azimuth rate using output of the tracker (which may or not have an associated contact at any given time) at the ping rate time interval. The discretized velocity and azimuth rate values are sorted into eleven and the seven bin histograms (Table I, features 15-25 and 26-32) respectively.

## 4 Feature generative processes

The generative processes for statistical modelling of a joint distribution of discrete aggregated features of multistatic sensors and kinematic tracking level features can be modelled in a framework of a Latent Dirichlet Allocation (Fig. 4). Originally LDA was mainly proposed for the probabilistic description of documents [8]. At present LDA provides a core algorithm for numerous text and image processing approaches.

We identify the multinomial features given in Table I as words drawn from a vocabulary of thirty two words ( $V = 32$ ). ‘‘Documents’’ are tracks each consisting of  $N_l$  estimated multinomial features  $w_{1:N_l}$ . Finally ‘‘topics’’ are virtual reflecting objects (VROs). We adopt the original LDA [8][9] for track feature generation description and assume a constant ( $K$ ) number of VROs labelled by tokens:  $z_n = \{1, \dots, K\}$ .

According to LDA (here redefined for the tracking framework), a track is a mixture of VROs, each VRO defining a distribution over features  $w$  (Fig. 4). The proportions of the mixture model  $\phi^j = P(w|z = j)$  are drawn on a track-specific basis from a Dirichlet distribution defined by a hyper-parameter  $\beta$  and refer to the multinomial distributions over features for the VRO token  $j$ . The multinomial distribution over VROs for track  $l$  is given by  $\theta^l = P(z)$ . Each feature  $w_i$  in a track is generated by first sampling a VRO from the VRO distribution, followed by sampling a feature from the VRO-feature distribution. In this way each feature is an independent and identical draw from a mixture

model conditioned on the mixing proportions and on the VRO

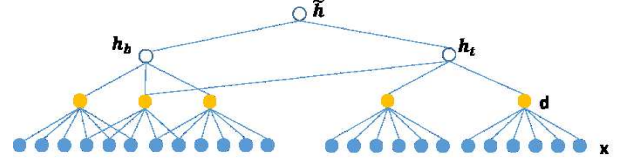


Fig. 3: a hierarchical view of estimation of low level features  $\mathbf{d}$  and  $\tilde{h}$ ;  $\mathbf{x}$  - normalized data snippets,  $\mathbf{d}$  – values of MMD test,  $\tilde{h}_b$  and  $\tilde{h}_t$  – across and along beam entropies of  $\mathbf{d}$  distributions,  $\tilde{h} = \tilde{h}_b - \tilde{h}_t$

token  $j$ .

Since distributions of VROs are unknown, the respective variables (i.e.  $\theta, \phi, z$ ) should be treated as the latent parameters that are to be inferred from data. Under the exchangeability assumption, the order of features in a track can be ignored.

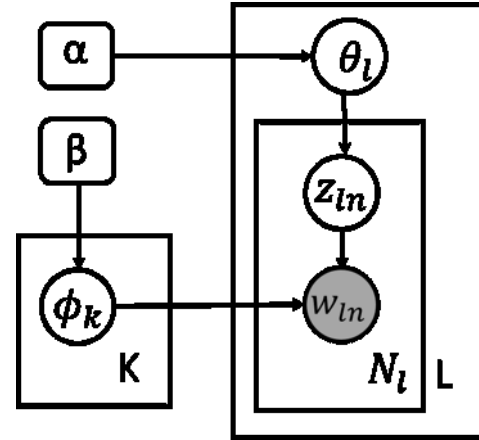


Fig. 4: Graphical model of VRO model in plate notation. The boxes represent replicates. The outer box on the right represent  $L$  tracks, the inner box represents the  $N_l$  samples of VROs and features within a track. The box on the right represents  $K$  VRO distributions. The shaded and unshaded variables indicate observed and unobserved variables respectively.

The model specifying the distribution over features within a track is given by [9]:

$$P(w_i) = \sum_{j=1}^K P(w_i|z_i = j)P(z_i = j) \quad (1)$$

As shown by [9], the VROs can be inferred using Gibbs sampling by considering each feature token in the track collection in turn, and estimating the probability of assigning the current feature token to each VRO, conditioned on the VRO assignments to all other feature tokens. The unnormalized probability of assigning a feature token to VRO  $j$  is calculated by (normalisation constant can be obtained summing the left side over all VROs):

$$P(z_i = j | \mathbf{z}_{-i}, w_i, l_i, \cdot) \propto \frac{c_{ij}^{VK} + \beta}{\sum_{w=1}^V c_{wj}^{VK} + V\beta} \frac{c_{dj}^{LK} + \alpha}{\sum_{t=1}^T c_{tj}^{LK} + K\alpha} \quad (2)$$

where  $C^{VK}$  and  $C^{LK}$  are matrices with dimensions  $V \times K$  and  $L \times K$  of feature and VRO counts assigned to  $j^{\text{th}}$  VRO and  $l^{\text{th}}$

track excluding respective current  $i^{\text{th}}$  instances,  $\mathbf{z}_{-i}$  refers to the VRO assignments of all feature tokens excluding  $i^{\text{th}}$  instance,  $z_i = j$  stays for the VRO assignment of token  $i$  to VRO  $j$ , and  $\dots$  refers to all other known information such as other feature and track indices  $\mathbf{w}_{-i}$  and  $\mathbf{l}_{-i}$ , and hyper-parameters  $\beta$  and  $\alpha$ .

Having direct estimates of  $z$  for each feature, we want to estimate  $\theta$  and  $\phi$  from the feature-VRO and VRO-track distributions respectively

$$\theta_{dj} = \frac{c_{dj}^{DK} + \alpha}{\sum_{k=1}^K c_{dk}^{DT} + T\alpha}; \quad \phi_{ij} = \frac{c_{ij}^{WK} + \beta}{\sum_{k=1}^W c_{kj}^{WT} + V\beta} \quad (3)$$

One can see that having a large collection of tracks, LDA can be used to discover track patterns cast as a posterior problem. We will see below that the hidden VRO and tracks structure can be visualized, and generalized to include new data into the structure in the future.

#### 4.1 Implementation of LDA inference

To demonstrate practical aspects of DPAT ambiguity reduction, we used basic Matlab LDA implementation as described in the Topic Modeling Toolbox (TMT) [10].

To infer the LDA structure we used Gibbs sampler specified by the Matlab function [10]:  $[\sim, \sim, Z] = \text{GibbsSamplerLDA}(W, D, K, N, \text{ALPHA}, \text{BETA}, \text{SEED}, \text{OUTPUT})$ . Here  $W$  and  $D$  contain the feature and track indices for the  $k^{\text{th}}$  token.  $K$  specifies the number of VROs,  $N$  defines the number of iterations to run the Gibb sampler,  $\text{ALPHA}$  and  $\text{BETA}$  are the hyper-parameters on the Dirichlet priors for the VRO distributions ( $\theta$ ) and the VRO feature distributions ( $\phi$ ) respectively,  $\text{SEED}$  is a variable used for Matlab random number initialization, and  $\text{OUTPUT}$  determines the screen output by the sampler. The output  $Z$  contains the inferred VRO assignments or tokens.

To demonstrate how  $W$  and  $D$  are formed in the context of this work, we first give a simplified example using only four features (i.e. a cardinality of vocabulary equals to four), the first one being  $\tilde{h}$  with two possible discrete values ( $\tilde{h}1, \tilde{h}2$ ) and the second velocity ( $v$ ) with a three possible values ( $v1, v2, v3$ ). By observing two tracks with the first track including two  $\tilde{h}1$  observations and one  $v3$  observation, and the second track including one  $\tilde{h}1$ , two  $\tilde{h}2$ , one  $v1$ , and two  $v2$  observations, we will have the following input vectors:

$$W=[1,1,5,1,2,3,4,4], \text{ and } D=[1,1,1,2,2,2,2];$$

## 5 Results

### 5.1 Data collection and processing

We use data of a field experiment during which multistatic acoustic data was collected in a geographical box of approximately 31 by 31 km by two AUVs operated either concurrently or sequentially for 5-8 hour a day for six days. The target that had to be detected by AUVs was an echo-repeater (ER). It was towed behind a vessel. Each day the ER was towed along approximately the same spatial pattern. The

source was a stationary source pinging on a regular time interval.

We first pre-processed all data collected by towed arrays of hydrophones, followed by estimation of the features described in Sections 3.2 and 3.3. The positions of the contacts for each source ping were estimated from the bistatic equations. The respective information was passed to the tracking algorithm. The parameters governing the tracking algorithm were kept constant through all experiments. As a result we obtained tracks, the contacts associated with the tracks, and the features on the contact and tracking levels. After rejecting tracks with duration shorter than five pings, the number of tracks and the number of feature tokens associated with tracks were equal to 331 tracks and 69614 token instances respectively (Table I).

As it was shown in the previous section, each track had associated with it a histogram of counts of the feature observations. To form a one dimensional feature vector  $WS$  required for the input of LDA algorithm, the respective histograms were ‘‘flattened’’ as shown in the 4.1 example.

After some experimentation we defined a number of VROs to be equal to four. This number is approximately consistent with the number of effective states of HMM used for classification of tracks in our previous work, and is useful for track visualisation. The input parameters were defined as follows:  $K=4$ ,  $N=3000$ ,  $\text{ALPHA}=0.3$ ,  $\text{BETA}=0.001$ ,  $\text{SEED}=30$ ,  $\text{OUTPUT}=1$ .

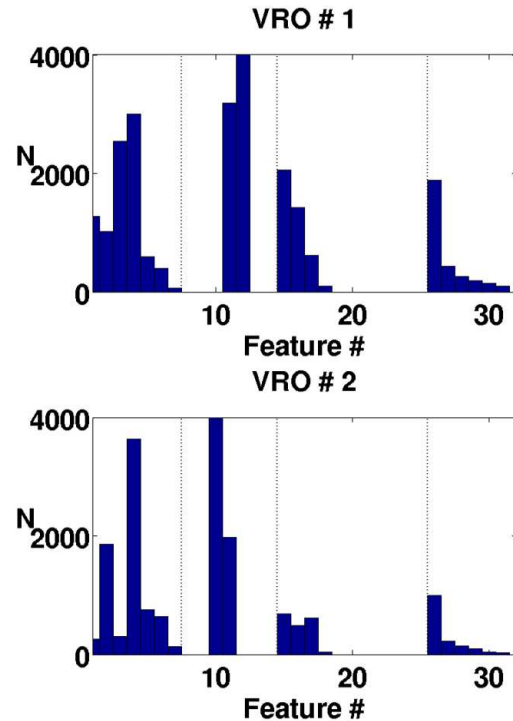


Fig. 5A: feature histograms for the Virtual Reflecting Objects 1 and 2

### 5.2 Analysis of VRO histograms

Feature histograms for each VRO are shown in Fig. 5A, 5B. Visual inspection of feature distributions shows:

- The features 8-14 corresponding to the MMD output show no changes for VRO#3 (i.e. only token 11 is observed). For other VROs the respective tokens are either {9, 10} or {10, 11}. It should be noted that although the range of MMD tokens may be increased by fine tuning the RBF scaling factor, it was not done in this work.
- The velocity distribution (features 15-25) is dominated by the low (relative to the BIN scale) velocities for VRO1 and 2, and by the medium to high velocities for VRO4.
- VRO1 and VRO4 exhibit comparable azimuth rate (features 26-32) distributions.
- Comparison of all VROs shows that DEST distribution (features 1-7) is the main factor contributing to the VROs' non-kinematic feature variability.

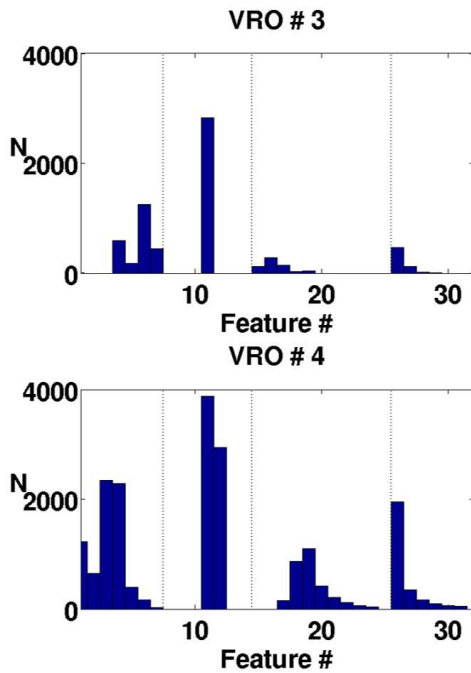


Fig. 5B: feature histograms for the Virtual Reflecting Objects 3 and 4.

### 5.3 Visualization of track patterns

Having obtained VRO assignments for each of the feature tokens input into the LDA algorithm, we counted how many times each VRO had been assigned to feature tokens in each track. By normalizing the respective histograms for each track we obtained the feature probability mass function (p.m.f.) estimates. The track p.m.f.'s were then used for clustering and visualization of tracks using two approaches. In the first approach we estimated the symmetric Kullback Leibler distances between tracks, followed by the classical

multidimensional scaling (MDS) estimation. The coordinates

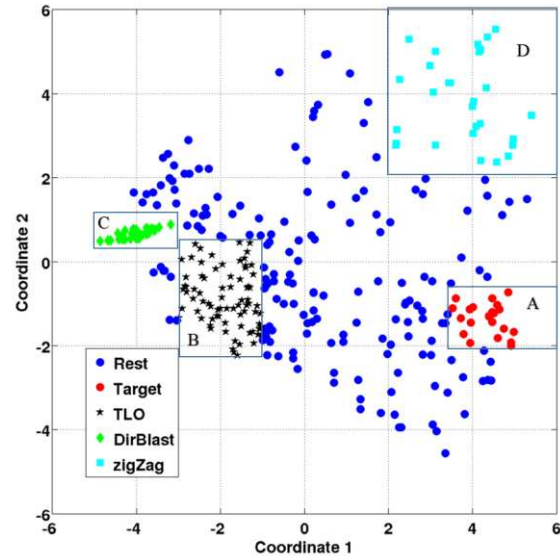


Fig. 6: distribution of tracks at the 2D output of multidimensional scaling track distance matrix. The tracks contained in boxes A-C correspond to four track classes as indicated by the legend.

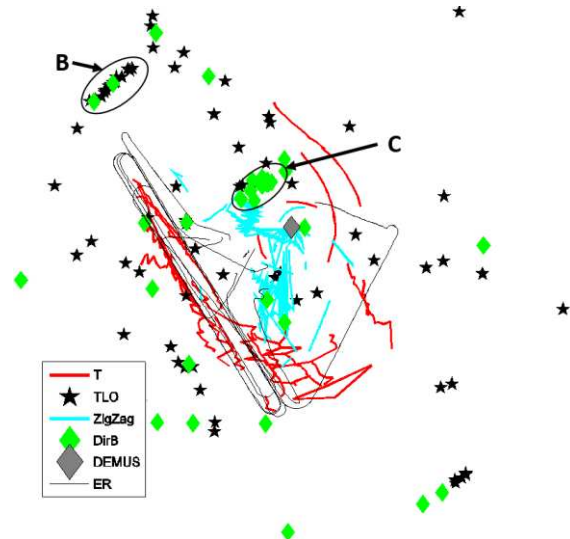


Fig. 7: distribution of tracks corresponding to the A-C boxes in Fig. 6. The median of track locations are shown for “DirBlast” and “TLO” classes. The markers with the highest spatial density are shown respectively by C and B ellipses. The “T” and “ZigZag” tracks are shown by solid thick lines. The ER trajectory is shown by thin black lines.

of the MDS output corresponding to the first two highest eigenvalues were then used to visualize patterns of track distribution (Fig. 6).

Since we did not have any ground truth information about TLO tracks, after some tests followed by visual inspection we identified three classes of the TLO tracks shown by the boxes A to D and labelled the respective tracks as T, TLO, DirBl,

and ZigZag (Fig. 6). The location and boundary values of these boxes are approximate and can be redefined when an increased amount of data and/or ground truth information becomes available. In this work the remaining part of tracks shown by the blue filled circles have been excluded from further analysis.

The Box C in the center of the left side of Fig. 6 corresponds to the dense area of tracks having contacts affected by sidelobes of direct blast (see also Fig. 7, here C indicates the area of increased density of the DirBl tracks). Many of these tracks were usually overlapping in a compact geographical area in the vicinity of the DEMUS source (denoted by the grey filled diamond, Fig. 7; note that contacts corresponding to the bistatic distances shorter than AUV – source distance were removed during preprocessing). We observed another geographical area (Box B, Fig. 6) not related to the direct blast but which also had many overlapping tracks (TLO) located within a relatively small area (B, Fig. 7). To show all these tracks in one figure without significantly increasing clutter, only median locations of the

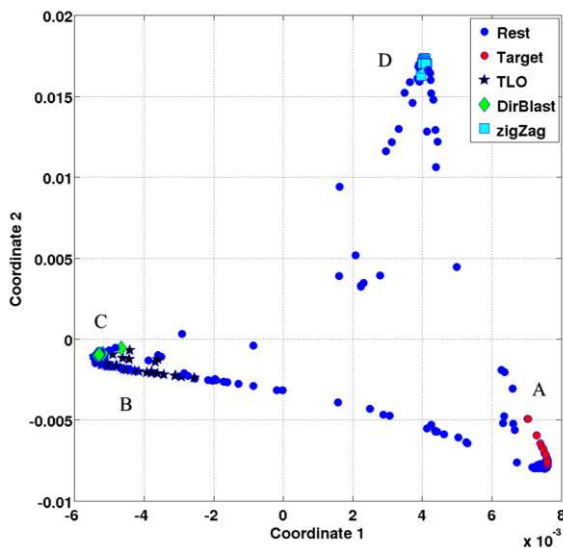


Fig. 8: distribution of tracks as a function of the first two KPCA components. The respective colours can be used to cross-reference the tracks of this figure and the tracks of Fig. 6

respective tracks are shown in Fig. 7. The rest of the DirBl and of the TLO tracks scattered within the area of observations were obviously defined by noise and/or reverberation.

Finally we observed the relatively long and straight tracks (the red lines of Fig. 7 corresponding to the A box of Fig. 6) aligned with the ER trajectory (the T tracks), and the tracks exhibiting zig-zag patterns (the ZigZag tracks).

The second visualization approach was based on kernel PCA. A track distribution plot obtained using the first two principle components of kernel PCA (Fig. 8) applied directly to the normalized histograms revealed a well pronounced triangular track distribution: the “A” box tracks corresponding to the target are located in the vicinity of the

lower-right corner of triangle, the ZigZag tracks are located at the top and the DirBlast and the TLO tracks in the left end of the triangle.

Having identified the A-C boxes, it is possible to compare the feature histograms based on the tracks found within these boxes. The histograms shown in Fig. 9 explain the KPCA results by identifying the three major VRO variance contributors: the T (Box A) – VRO 4, the DirBl (Box B), the TLO (Box C) – VRO 1, and the ZigZag (Box D) – VRO 2 track classes. Note that the main difference between VRO1 and VRO4 lies in the frequency distribution of velocities: for the VRO #1 the contribution of respective tokens is relatively high for  $0 < v < 1$  m/s with no contribution for  $v > 1.5$  m/s. At the same time, for VRO#4, the tokens corresponding to  $v > 1.5$  are dominating with no or negligible contribution for  $v < 1.0$  m/s.

## 6 Summary

We have shown that in a high false track rate scenario, which is typical to multistatic networks in coastal areas, the ambiguity of target detections can be significantly reduced

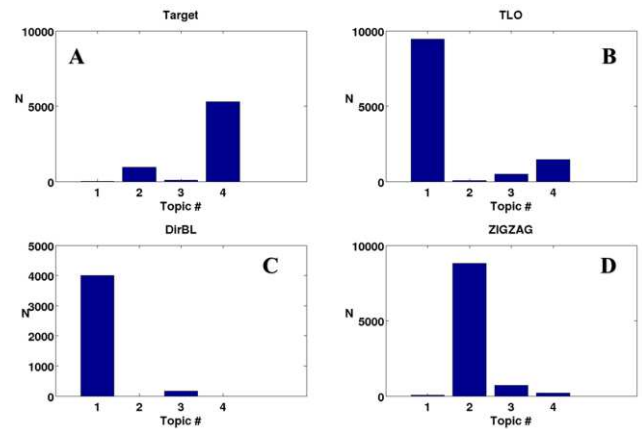


Fig.9: Histograms showing contribution of VROs (topics) to the T, TLO, DirBl and ZigZag classes of boxes A,B,C, and D in Fig.6 respectively.

through the learning of track clusters directly from data. Uncertainty of track and contact labelling dictates the requirement for formation of track clusters such that they can be labelled using uncertain ground truth information.

A combination of the aggregated discriminative low-level features and the high level kinematic features proposed in this work makes track clustering possible within a framework of topic modelling. This result also makes possible supervised track classification in the future.

Although for autonomous systems DPAT has to be fully automatic, human input is required for the final decision in most of present day operations. For this reason, interpretability of information used for human decision making is very important. The LDA framework can provide such an interpretation and depends to a large extent on the interpretability of features or words, and VROs or topics.

## 7 Appendix: MMD Test

The MMD test is performed on a pair of interleaved bearing-time cells in a time-bearing (TB) window (TBW) with a predefined non-dimensional range  $N = \lfloor f_s R / (2c) \rfloor$ , (where  $f_s$  is the normalized data sampling frequency,  $R$  is the expected length of target, and  $c$  is sound speed) and number of beams ( $M = 3$ ) support (for more details see [3]). We apply this test to quantify dissimilarity of the interleaving TB cells.

An empirical biased estimate of MMD defined for the pair of TB cells  $\hat{X}$  and  $\tilde{X}$  (in Fig. 2 shown respectively by the red and green boxes) in the TBW can be written as [8]

$$d[\hat{X}, \tilde{X}] = \frac{1}{M^2} \left[ \sum_{s,o}^M k(\hat{x}_s, \hat{x}_o) - 2 \sum_{s,o}^M k(\hat{x}_s, \tilde{x}_o) + \sum_{s,o}^M k(\tilde{x}_s, \tilde{x}_o) \right], \quad (5)$$

where  $M$  correspond to the numbers of beams in the TB window,  $k(\hat{x}_s, \tilde{x}_o)$  is a kernel function,  $\hat{x}_s$  and  $\tilde{x}_o$  are renormalized (the first normalization is a part of data preprocessing) vectors of the TBW cells respectively at beams  $s$  and  $o$ , ( $\tilde{x}_o = \tilde{x}_o^* / \|\tilde{x}_o^*; \hat{x}_o^*\|$  and  $\hat{x}_o = \hat{x}_o^* / \|\tilde{x}_o^*; \hat{x}_o^*\|$ ) respectively, where  $[\tilde{x}_o^*; \hat{x}_o^*]$  stays for concatenation of normalized time snippets at the beam  $o$ ). We used the Gaussian radial basis function (RBF)  $k(\hat{x}_s, \tilde{x}_o) = \exp(-\|\hat{x}_s - \tilde{x}_o\|^2 / \sigma^2)$ , where  $\sigma^2$  is a scaling parameter that after some testing was set to 0.01. We discretize the output of MMD test  $d_{j=i} = \min_i |d_i - (1 - \sqrt{d})|$  on -2 to 2 interval with the grid step 0.1

The discretized MMD values estimated along the beam of contact (e.g. beam  $j=4$ , time indices  $i = \{2, \dots, 6\}$  in Fig. 2A) correspond to the features 8-14 in Table 1. The three bin MMD histograms  $p(d_r) = W_r / M$ , such that  $\sum_{r=1}^M p_r(d_r) = 1$ ,  $\sum_{r=1}^M p_b(d_r) = 1$  where  $W_r$  is the number of  $d_r$  values (counted either in  $\{d_{i-1,j}, d_{i,j}, d_{i+1,j}\}$  or in  $\{d_{i,j-1}, d_{i,j}, d_{i,j+1}\}$ ) falling within the  $r^{\text{th}}$  bin that are estimated using three MMD values taken along ( $d_\tau = \{d_{i-1,j}, d_{i,j}, d_{i+1,j}\}$ ), and three MMD values taken across ( $d_b = \{d_{i,j-1}, d_{i,j}, d_{i,j+1}\}$ ). The respective entropies are estimated using

$$h_\tau = -\sum_{r=1}^M p_r(d_r) \log p_r(d_r), \text{ and}$$

$$h_b = -\sum_{r=1}^M p_b(d_r) \log p_b(d_r).$$

## References

[1] T.K. Stanton, D. Chu, J.M. Gelb, G.L. Tipple, "Interpreting Echo Statistics of Three Distinct Clutter Classes Measured With a Midfrequency Active Sonar: Accounting for Number of Scatterers, Scattering Statistics, and Beam pattern Effects", *J. Oceanic Engineering*, vol. PP, pp. 1-9, 2014.

[2] P. Braca, R. Goldhahn, K. LePage, S. Marano, V. Matta and P. Willett, "Cognitive Multistatic AUV Networks", *Proc. of the 17th International Conference on Information Fusion (FUSION 2014)*, Salamanca 2014.

[3] J.Sildam, P. Braca, K.D. LePage, and P. Willett, "Unsupervised Track Classification Based on

Hierarchical Dirichlet Processes", in *Proc. of the 21th European Signal Processing Conference 2013 (EUSIPCO 2013)*, Marrakesh 2013.

[4] C. M. Payne, "Principles of Naval Weapon Systems, 2nd ed., Annapolis," USA: Naval Institute Press, 2006, p. 179.

[5] S. Dugelay, D.A. Abraham, "Reduction of Low Frequency Active Sonar Clutter Through Image Processing", *CMRE*, 1997, SR-272-UU.

[6] Gretton, A., Borgwardt, K. M., Rasch, M. J., Schölkopf, B. and Smola, A. J. "A Kernel Two-Sample Test," *Journal of Machine Learning Research*, 723-773, 13 (2012).

[7] J. Sildam, "Masking of Time-Frequency Patterns in Applications of Passive Underwater Target Detection", *EURASIP J. on Advances in Signal Processing*, vol. 2010, Jan. 2010.

[8] D. M. Blei, Andrew Y. Ng, and Michael I. Jordan. 2003. "Latent dirichlet allocation", *J. Mach. Learn. Res.* 3, 2003, pp. 993-1022.

[9] T. Griffiths, and M. Steyvers, "Finding Scientific Topics", *Proc. of the National Academy of Sciences*, 101 (suppl. 1), pp. 5228-5235, 2004.

[10] M. Steyvers, and T. Griffiths, Online, Matlab Topic Modeling Toolbox 1.4.

[11] A.N. Steinberg, and C.L. Bowman, "Revisions to the JDL Data Fusion Model", chapter.2, in. "Handbook of Multisensor Data Fusion", CRC Press, June 2001.

[12] G.T. Toussaint, "The Use of Context in Pattern Recognition," *Pattern Recognition*, vol. 10, 1977, pp. 189–204.

# Document Data Sheet

<i>Security Classification</i>		<i>Project No.</i>
<i>Document Serial No.</i> CMRE-PR-2019-106	<i>Date of Issue</i> June 2019	<i>Total Pages</i> 8 pp.
<i>Author(s)</i> Jüri Sildam, Kevin D. LePage		
<i>Title</i> Ambiguity reduction of underwater targets in framework of topic modeling		
<i>Abstract</i> <p>An unsupervised track classification approach based on appropriate discriminative and aggregative features derived from beamformed and normalized matched-filtered data is applied to sonar multistatic tracking and extended to include discretised track velocity and heading rate. A clustering algorithm based on the Latent Dirichlet Allocation model is proposed. It is demonstrated how low-level, highly variable and non-stationary data components can be combined through an increased abstraction level with higher level kinematic tracking features. Improved discrimination of tracks associated with both stationary and moving scatterers is demonstrated.</p>		
<i>Keywords</i> Multistatic tracking, data aggregation and clustering, track classification, Latent Dirichlet Allocation		
<i>Issuing Organization</i> NATO Science and Technology Organization Centre for Maritime Research and Experimentation Viale San Bartolomeo 400, 19126 La Spezia, Italy  [From N. America: STO CMRE Unit 31318, Box 19, APO AE 09613-1318]		Tel: +39 0187 527 361 Fax: +39 0187 527 700  E-mail: <a href="mailto:library@cmre.nato.int">library@cmre.nato.int</a>